

000	054
001	055
002	056
003	057
004	Supplementary Material to “External Prior Guided Internal Prior Learning for
005	Real Noisy Image Denoising”
006	058
007	059
008	060
009	061
010	062
011	Anonymous CVPR submission
012	063
013	Paper ID 1047
014	064
015	In this supplementary material, we provide:
016	1. The closed-form solution of the sparse coding problem (6) in the main paper.
017	2. More denoising results on the real noisy images in dataset [1].
018	3. More denoising results on the 15 cropped real noisy images (with mean image of 500 shots as “ground truth”) in dataset
019	[2].
020	4. More denoising results on the 60 cropped real noisy images (with mean image of 500 shots as “ground truth”) from
021	dataset [2].
022	<b>1. Closed-Form Solution of the Weighted Sparse Coding Problem (6)</b>
023	For notation simplicity, we ignore the indices $n, m, t$ in problem (6) of the main paper. It turns into the following weighted
024	sparse coding problem:
025	$\min_{\alpha} \ \mathbf{y} - \mathbf{D}\alpha\ _2^2 + \sum_{j=1}^{3p^2} \lambda_j  \alpha_j . \quad (1)$
026	Since $\mathbf{D}$ is an orthogonal matrix, problem (1) is equivalent to
027	$\min_{\alpha} \ \mathbf{D}^T \mathbf{y} - \alpha\ _2^2 + \sum_{j=1}^{3p^2} \lambda_j  \alpha_j . \quad (2)$
028	For simplicity, we denote $\mathbf{z} = \mathbf{D}^T \mathbf{y}$ . Here we have $\lambda_j > 0, j = 1, \dots, 3p^2$ , then problem (2) can be written as
029	$\min_{\alpha} \sum_{j=1}^{3p^2} ((\mathbf{z}_j - \alpha_j)^2 + \lambda_j  \alpha_j ). \quad (3)$
030	The problem (3) is separable w.r.t. each $\alpha_j$ and hence can be simplified to $3p^2$ independent scalar minimization problems
031	$\min_{\alpha_j} (\mathbf{z}_j - \alpha_j)^2 + \lambda_j  \alpha_j , \quad (4)$
032	where $j = 1, \dots, 3p^2$ . Taking derivative of $\alpha_j$ in problem (4) and setting the derivative to be zero. There are two cases for the
033	solution.
034	(a) If $\alpha_j \geq 0$ , we have
035	$2(\alpha_j - \mathbf{z}_j) + \lambda_j = 0. \quad (5)$
036	The solution is
037	$\hat{\alpha}_j = \mathbf{z}_j - \frac{\lambda_j}{2} \geq 0. \quad (6)$
038	So $\mathbf{z}_j \geq \frac{\lambda_j}{2} > 0$ , and the solution $\hat{\alpha}_j$ can be written as
039	$\hat{\alpha}_j = \text{sgn}(\mathbf{z}_j) * ( \mathbf{z}_j  - \frac{\lambda_j}{2}), \quad (7)$
040	where $\text{sgn}(\bullet)$ is the sign function.
041	(b) If $\alpha_j < 0$ , we have
042	$2(\alpha_j - \mathbf{z}_j) - \lambda_j = 0. \quad (8)$
043	The solution is
044	$\hat{\alpha}_j = \mathbf{z}_j + \frac{\lambda_j}{2} < 0. \quad (9)$

108 So  $\mathbf{z}_j < -\frac{\lambda_j}{2} < 0$ , and the solution  $\hat{\alpha}_j$  can be written as  
 109

$$\hat{\alpha}_j = \text{sgn}(\mathbf{z}_j) * (-\mathbf{z}_j - \frac{\lambda_j}{2}) = \text{sgn}(\mathbf{z}_j) * (|\mathbf{z}_j| - \frac{\lambda_j}{2}). \quad (10)$$

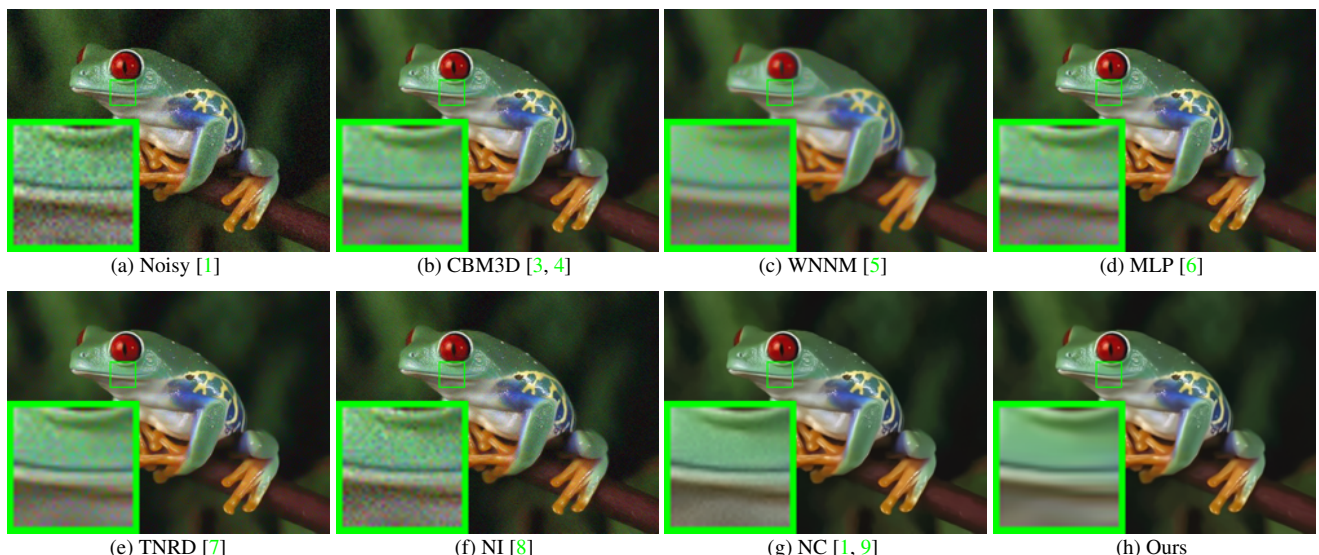
110 In summary, we have the final solution of the weighted sparse coding problem (1) as  
 111

$$\hat{\alpha} = \text{sgn}(\mathbf{D}^T \mathbf{y}) \odot \max(|\mathbf{D}^T \mathbf{y}| - \boldsymbol{\lambda}, 0), \quad (11)$$

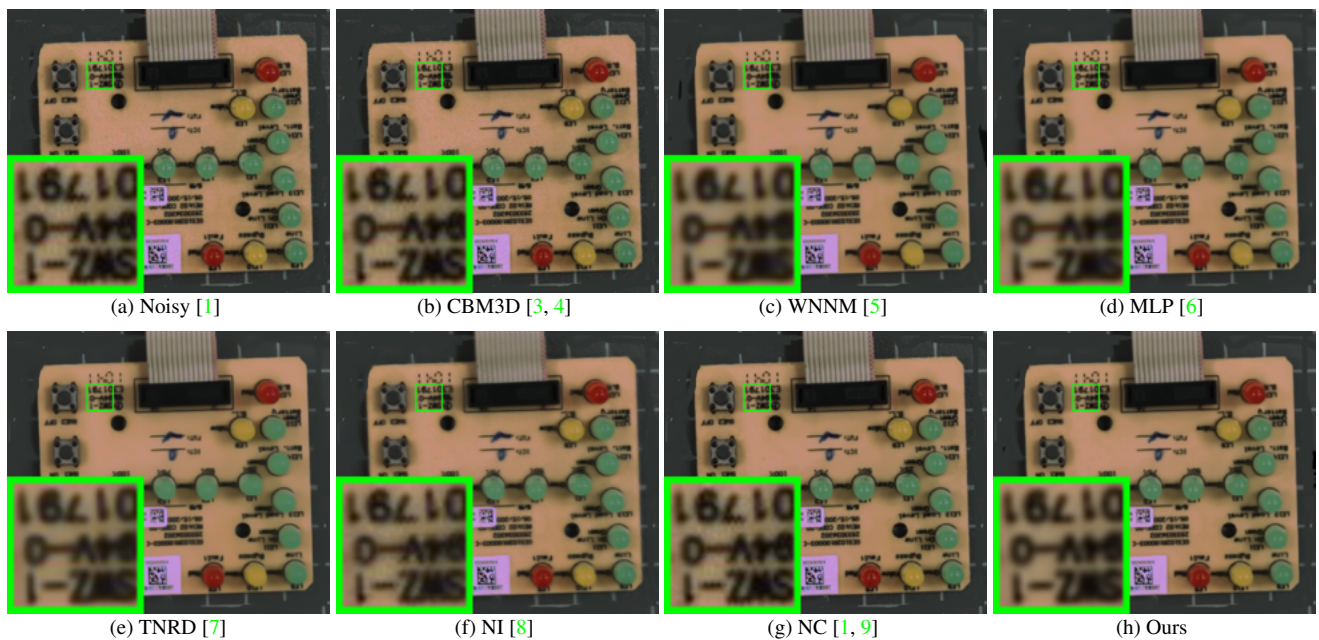
112 where  $\boldsymbol{\lambda} = \frac{1}{2}[\lambda_1, \lambda_2, \dots, \lambda_{3p^2}]^\top$  is the vector of regularization parameter and  $\odot$  means element-wise multiplication.  
 113

## 114 2. More Results on Real Noisy Images in [1]

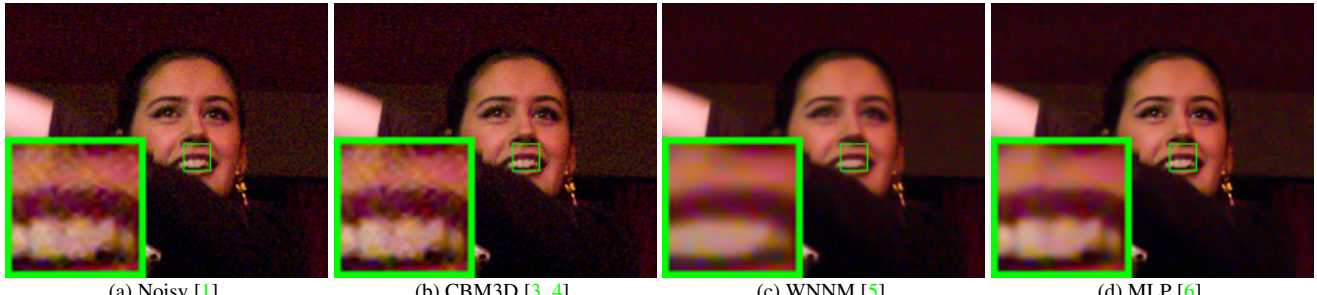
115 In this section, we give more comparisons of the competing methods on the dataset [1]. The real noisy images in dataset  
 116 [1] have no “ground truth” images and hence we only compare the visual quality of the denoised images by different methods.  
 117 As can be seen from Figures 1-4, our proposed method performs better than the state-of-the-art denoising methods.  
 118



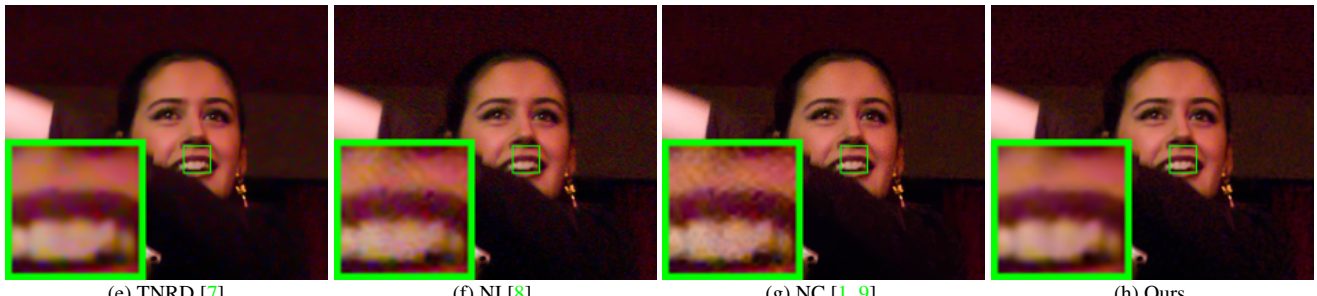
119 Figure 1. Denoised images of the real noisy image “Frog” [1] by different methods. The images are better to be zoomed in on screen.  
 120



121 Figure 2. Denoised images of the real noisy image “Circuit” [1] by different methods. The images are better to be zoomed in on screen.  
 122

216  
217  
218  
219  
220  
221  
222  
223  
224  
225  
226

(a) Noisy [1] (b) CBM3D [3, 4] (c) WNNM [5] (d) MLP [6]

227  
228  
229  
230  
231  
232  
233  
234  
235  
236

(e) TNRD [7] (f) NI [8] (g) NC [1, 9] (h) Ours

237  
238

Figure 3. Denoised images of the real noisy image “Woman” [1] by different methods. The images are better to be zoomed in on screen.

239  
240  
241  
242  
243  
244  
245  
246  
247  
248  
249

(a) Noisy [1] (b) CBM3D [3, 4] (c) WNNM [5] (d) MLP [6]

250  
251  
252  
253  
254  
255  
256  
257  
258  
259

(e) TNRD [7] (f) NI [8] (g) NC [1, 9] (h) Ours

260  
261  
262

### 3. More Results on the 15 Cropped Images Used in [2]

263  
264  
265  
266  
267  
268  
269

In this section, we provide more visual comparisons of the proposed method with the state-of-the-art denoising methods on the 15 cropped real noisy images used in [2]. In this dataset, each scene was shot 500 times under the same camera and camera setting. The mean image of the 500 shots is roughly taken as the “ground truth”, with which the PSNR can be computed. As can be seen from Figures 5-9, in most cases, our proposed method achieves better performance than the competing methods. This validates the effectiveness of our proposed external prior guided internal prior learning framework for real noisy image denoising.

270  
271  
272  
273  
274  
275  
276  
277  
278  
279  
280  
281  
282  
283  
284  
285  
286  
287  
288  
289  
290  
291  
292  
293  
294  
295  
296  
297  
298  
299  
300  
301  
302  
303  
304  
305  
306  
307  
308  
309  
310  
311  
312  
313  
314  
315  
316  
317  
318  
319  
320  
321  
322  
323

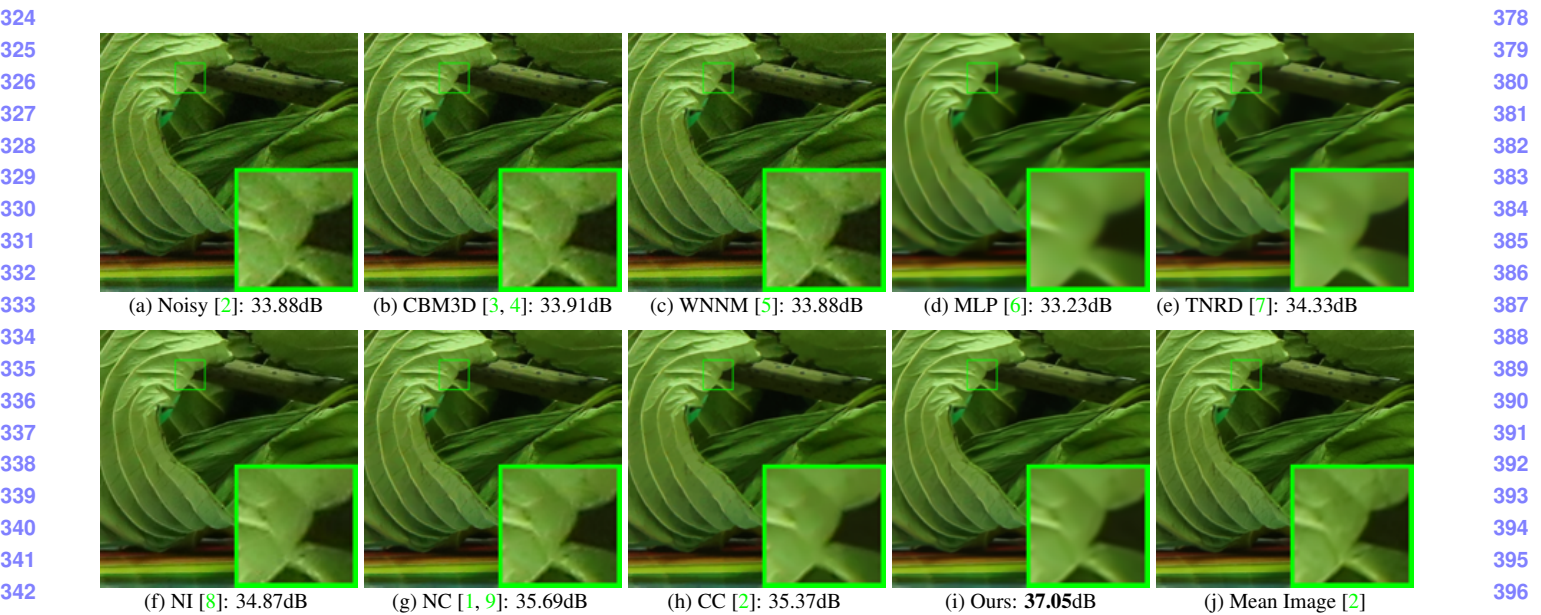


Figure 5. Denoised images of a region cropped from the real noisy image “Canon 5D Mark 3 ISO 3200 2” [2] by different methods. The images are better to be zoomed in on screen.

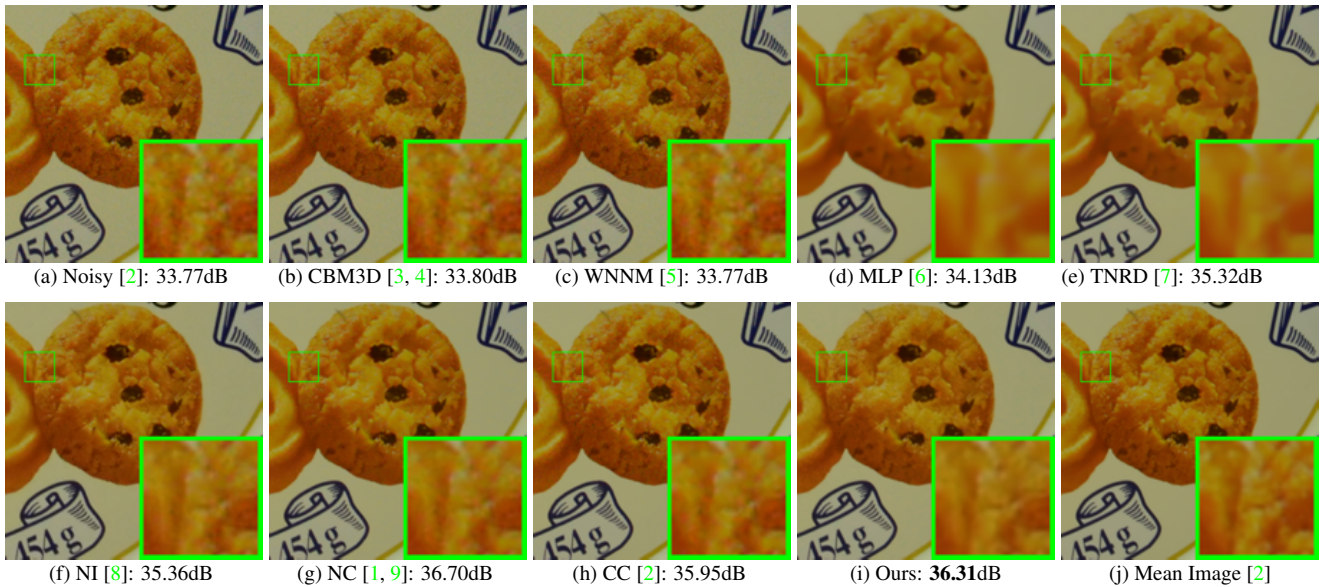


Figure 6. Denoised images of a region cropped from the real noisy image “Canon 5D Mark 3 ISO 3200 2” [2] by different methods. The images are better to be zoomed in on screen.

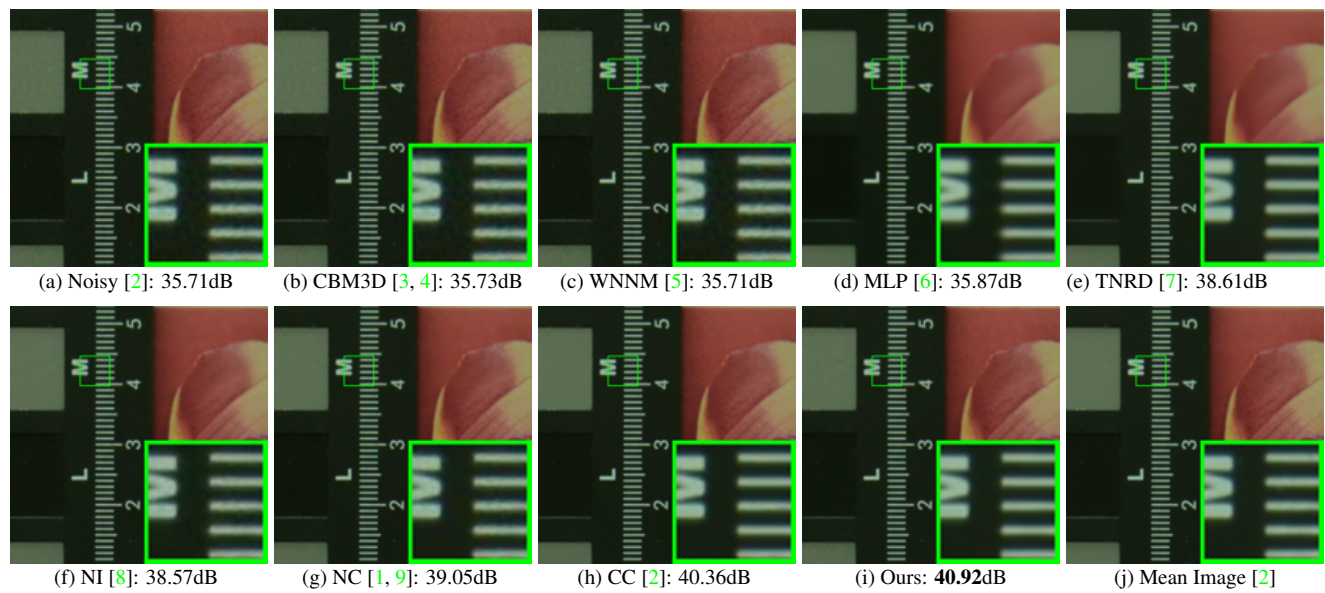


Figure 7. Denoised images of a region cropped from the real noisy image “Nikon D800 ISO 1600 2” [2] by different methods. The images are better to be zoomed in on screen.

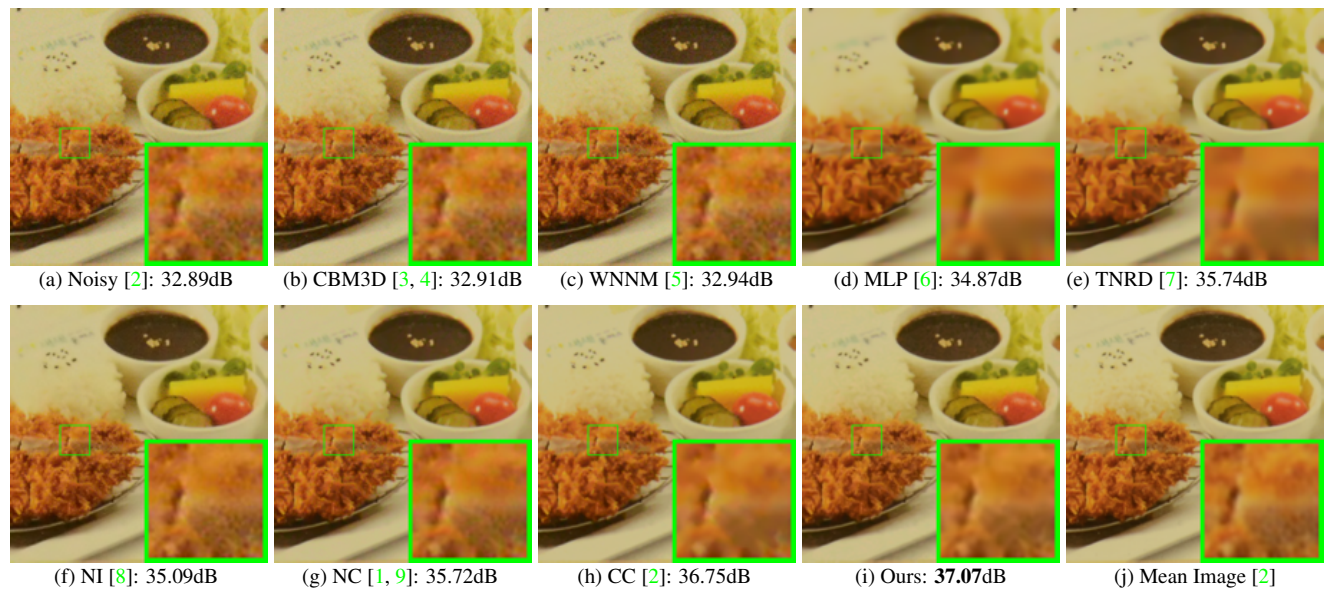


Figure 8. Denoised images of a region cropped from the real noisy image “Nikon D800 ISO 3200 2” [2] by different methods. The images are better to be zoomed in on screen.

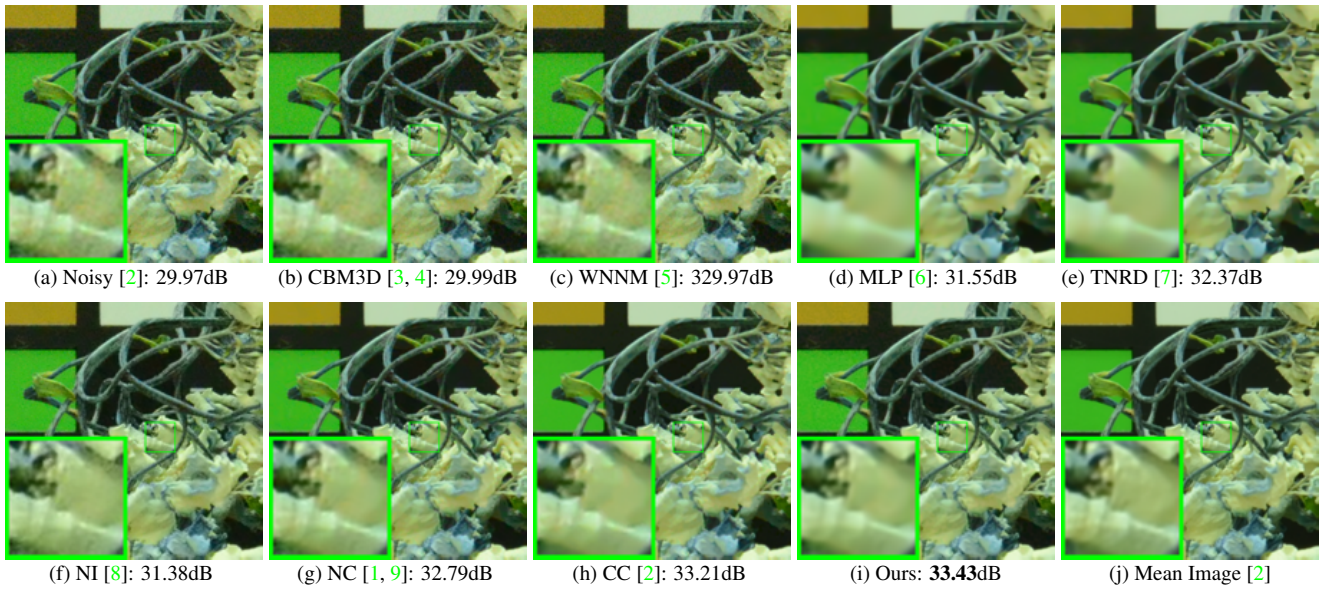


Figure 9. Denoised images of a region cropped from the real noisy image “Nikon D800 ISO 6400 2” [2] by different methods. The images are better to be zoomed in on screen.

#### 4. More Results on the 60 Cropped Images in [2]

In this section, we provide more visual comparisons of the proposed method with the state-of-the-art denoising methods on the 60 cropped real noisy images we cropped from [2]. As can be seen from Figures 10-20, on most cases, our proposed method achieves better performance than the competing methods. This validates the effectiveness of our proposed external prior guided internal prior learning framework for real noisy image denoising.

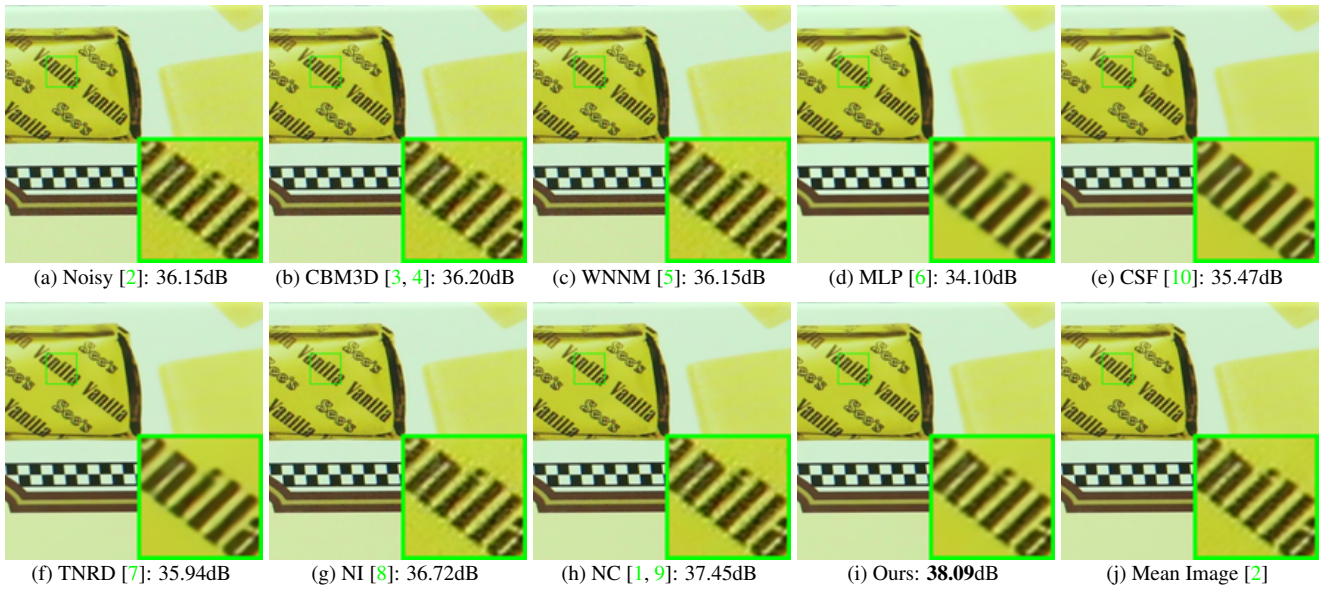


Figure 10. Denoised images of a region cropped from the real noisy image “Canon EOS 5D Mark3 ISO 3200 C1” [2] by different methods. The images are better viewed by zooming in on screen.

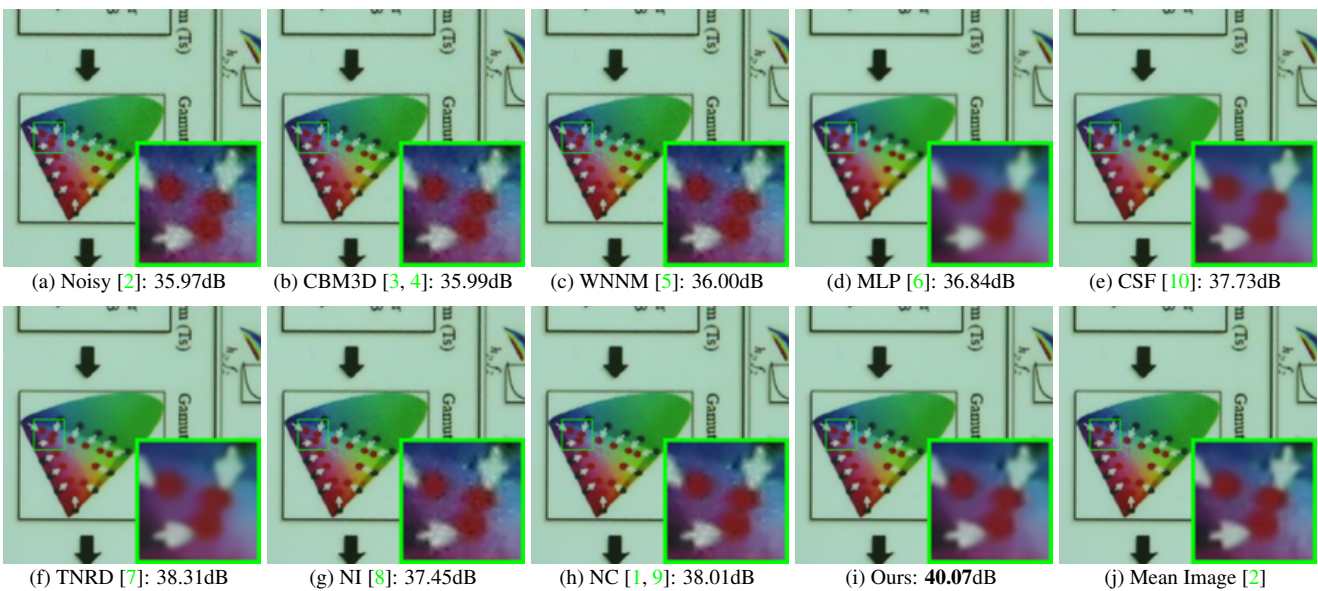


Figure 11. Denoised imagesupp of a region cropped from the real noisy image “Canon EOS 5D Mark3 ISO 3200 C2” [2] by different methods. The images are better viewed by zooming in on screen.

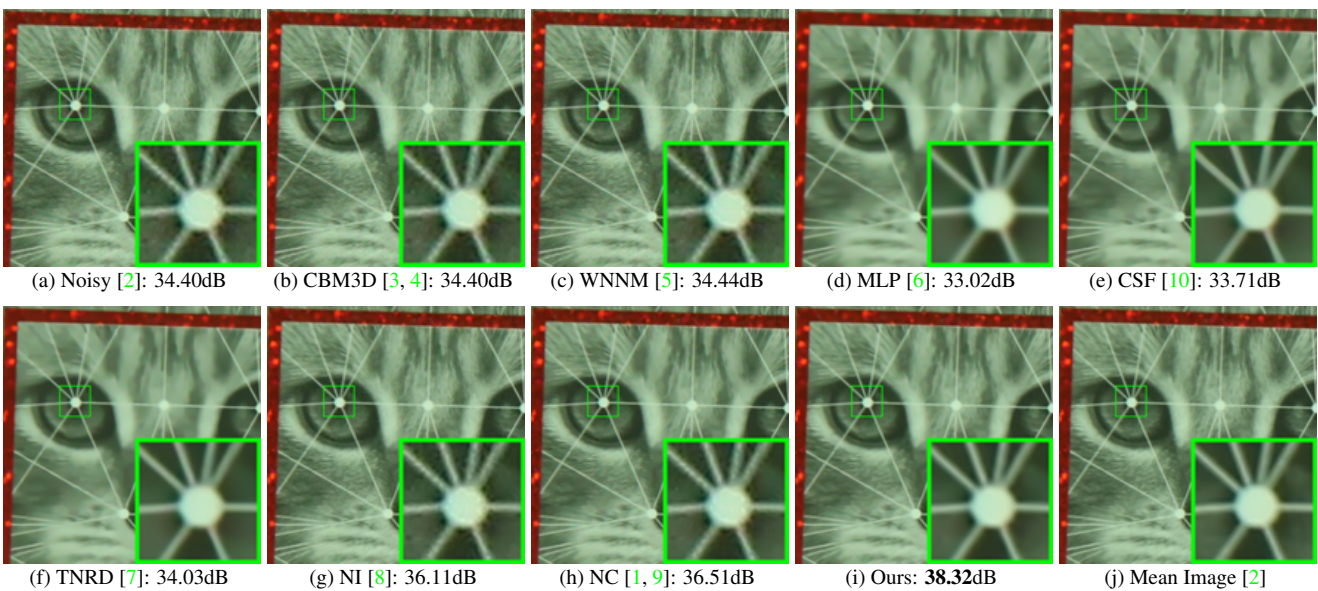


Figure 12. Denoised imagesupp of a region cropped from the real noisy image “Canon EOS 5D Mark3 ISO 3200 C3” [2] by different methods. The images are better viewed by zooming in on screen.

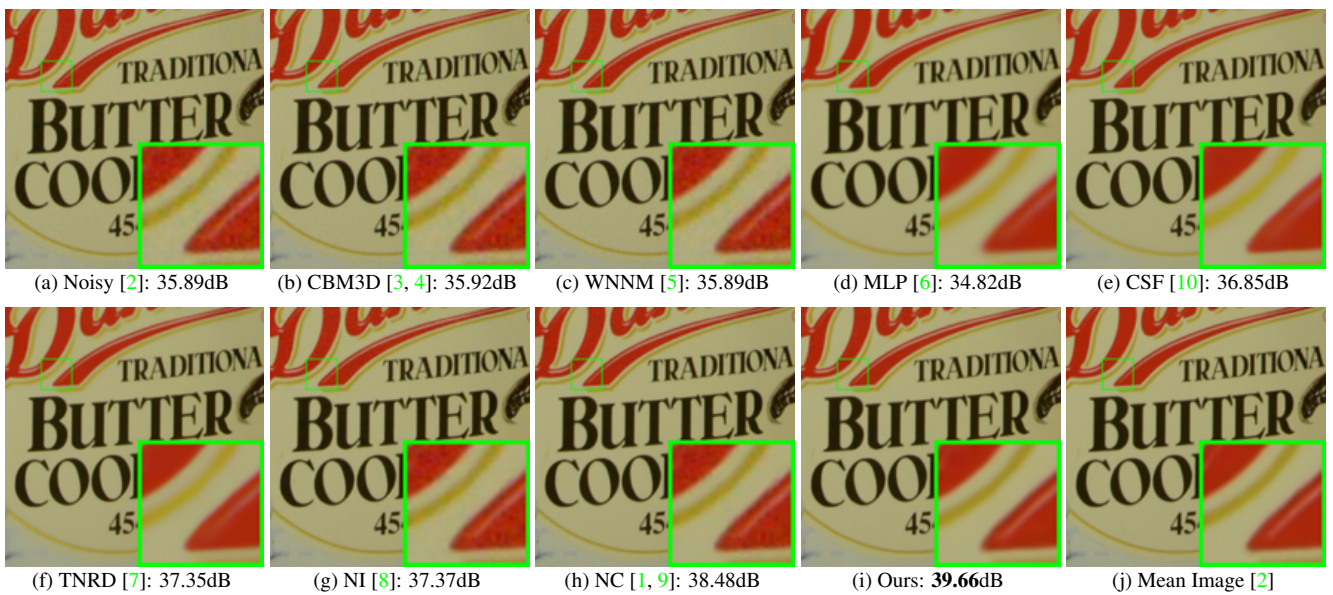


Figure 13. Denoised imagesupp of a region cropped from the real noisy image “Nikon D600 ISO 3200 C1” [2] by different methods. The images are better viewed by zooming in on screen.

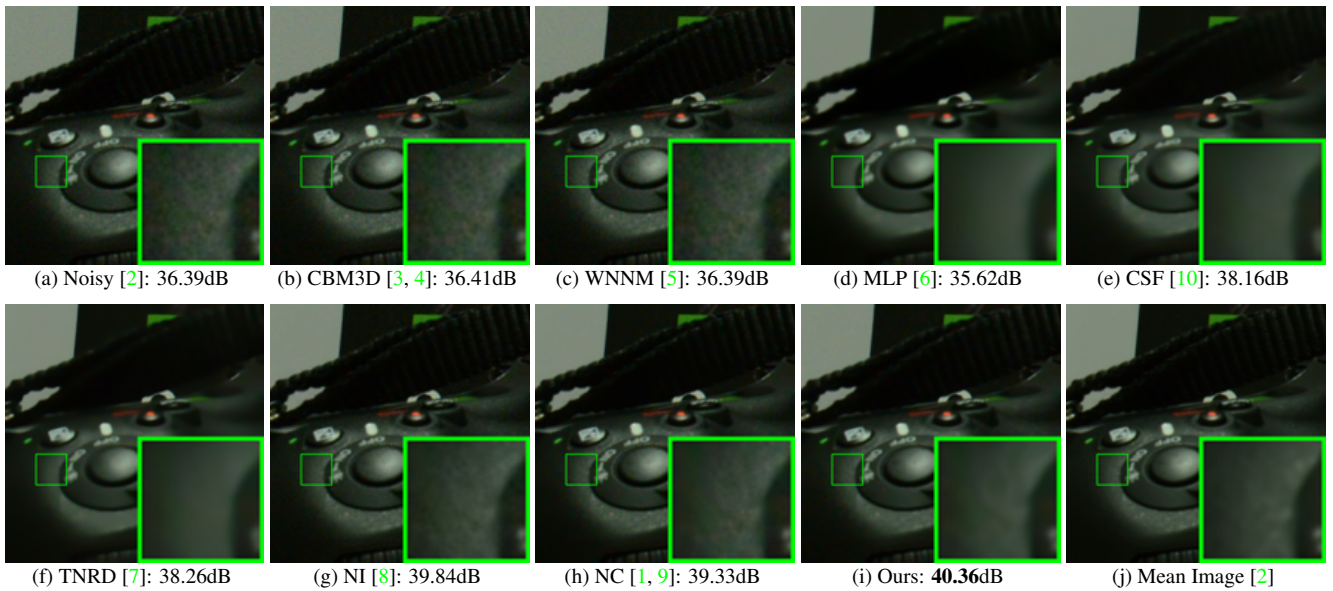


Figure 14. Denoised imagesupp of a region cropped from the real noisy image “Nikon D600 ISO 3200 C2” [2] by different methods. The images are better viewed by zooming in on screen.

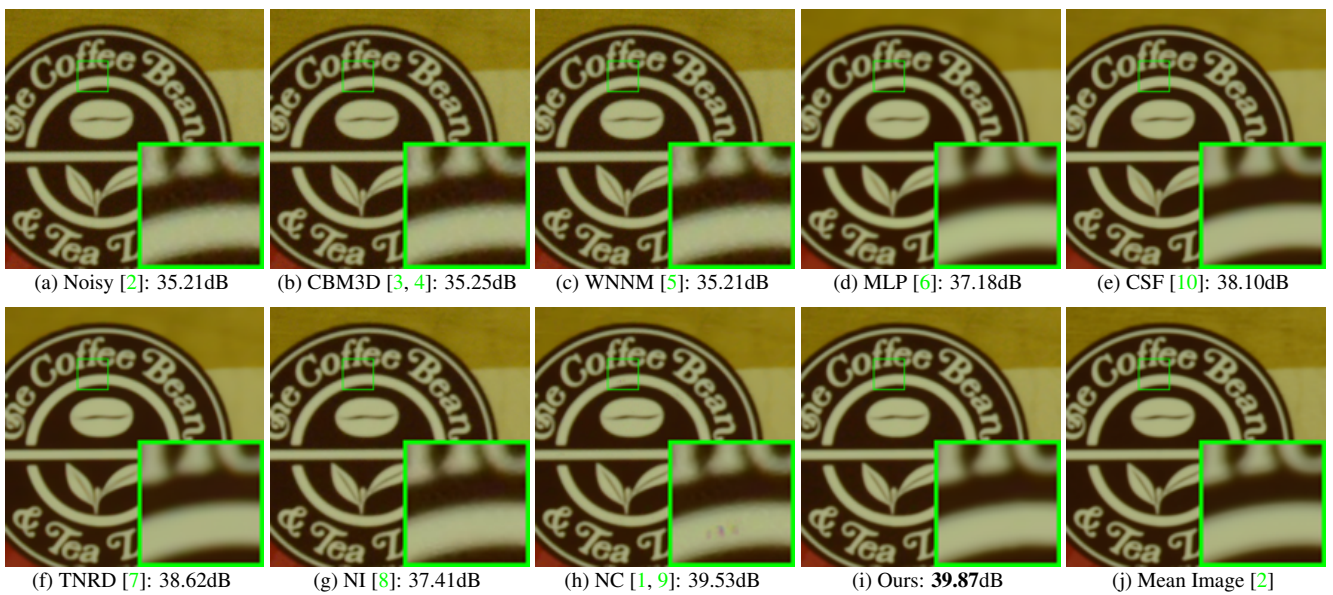


Figure 15. Denoised imagesupp of a region cropped from the real noisy image “Nikon D800 ISO 1600 B2” [2] by different methods. The images are better viewed by zooming in on screen.

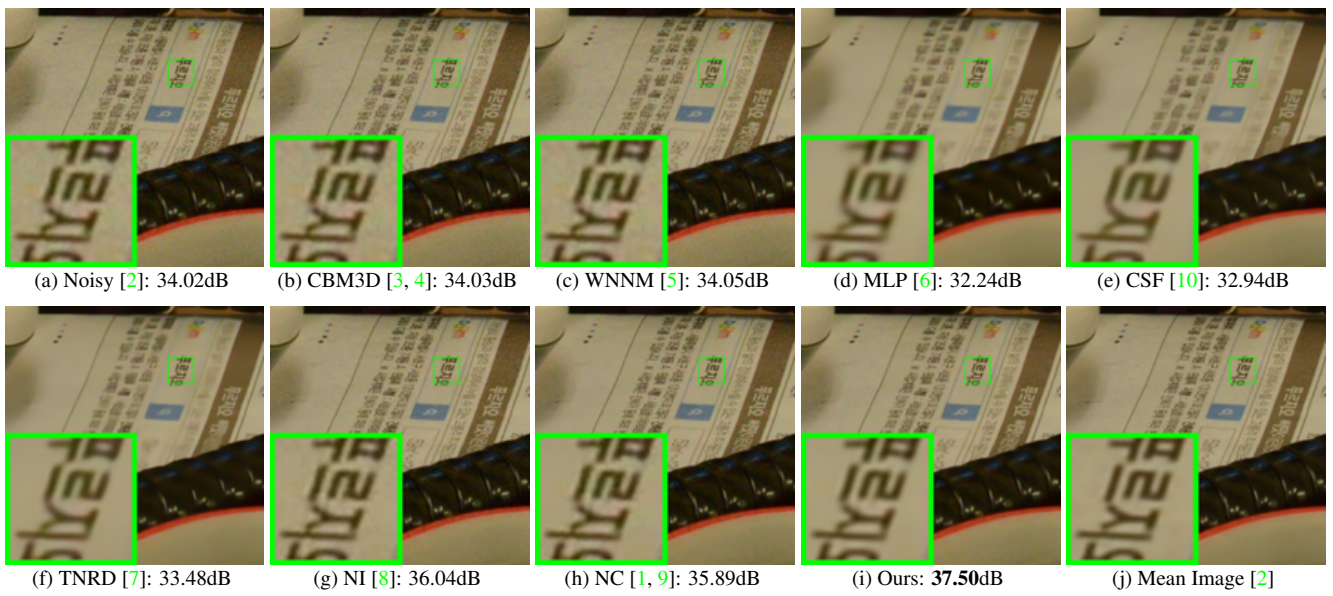


Figure 16. Denoised imagesupp of a region cropped from the real noisy image “Nikon D800 ISO 3200 A1” [2] by different methods. The images are better viewed by zooming in on screen.

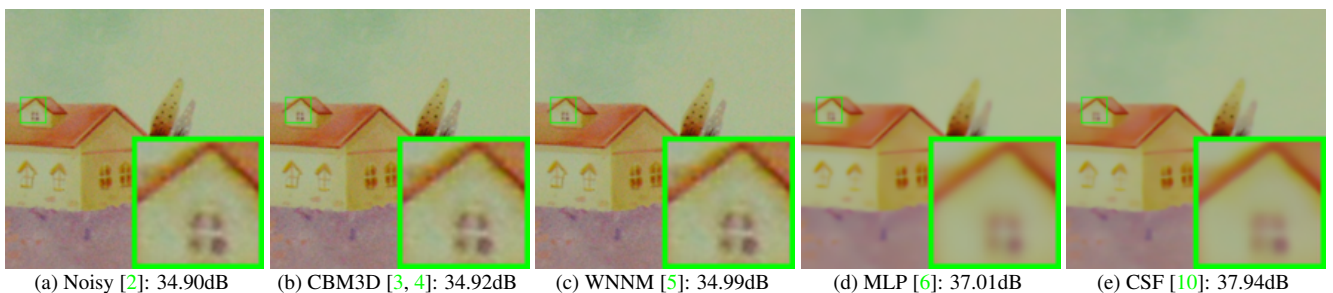


Figure 17. Denoised imagesupp of a region cropped from the real noisy image “Nikon D800 ISO 3200 A2” [2] by different methods. The images are better viewed by zooming in on screen.

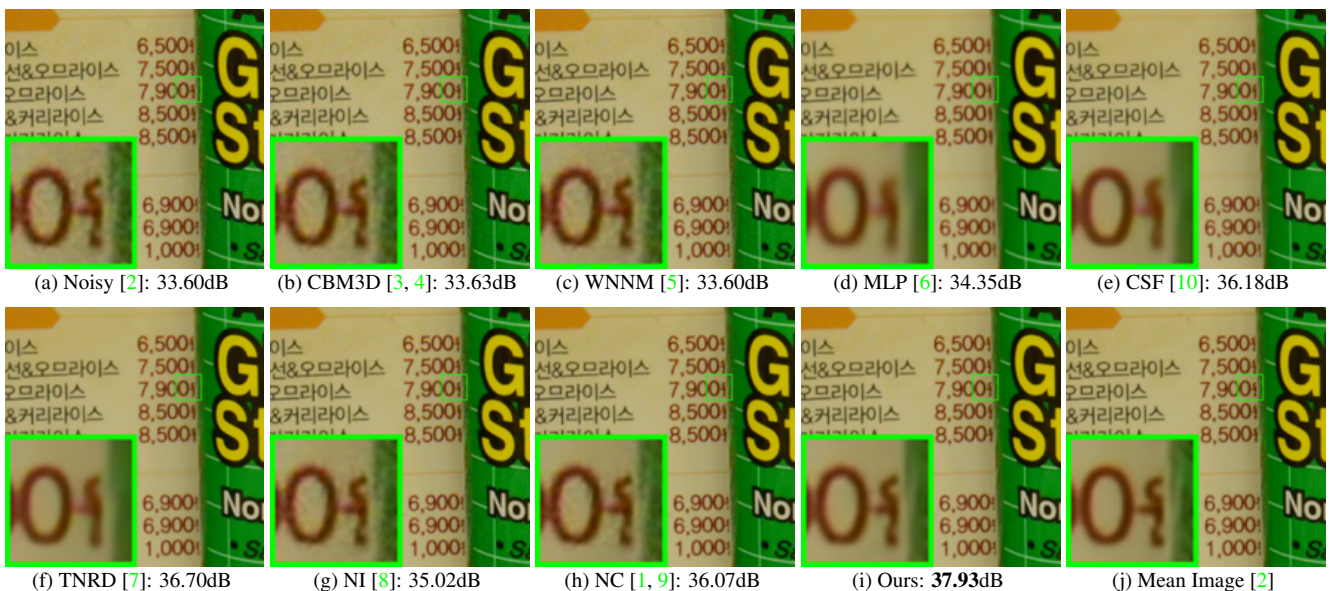


Figure 18. Denoised imagesupp of a region cropped from the real noisy image “Nikon D800 ISO 3200 A3” [2] by different methods. The images are better viewed by zooming in on screen.

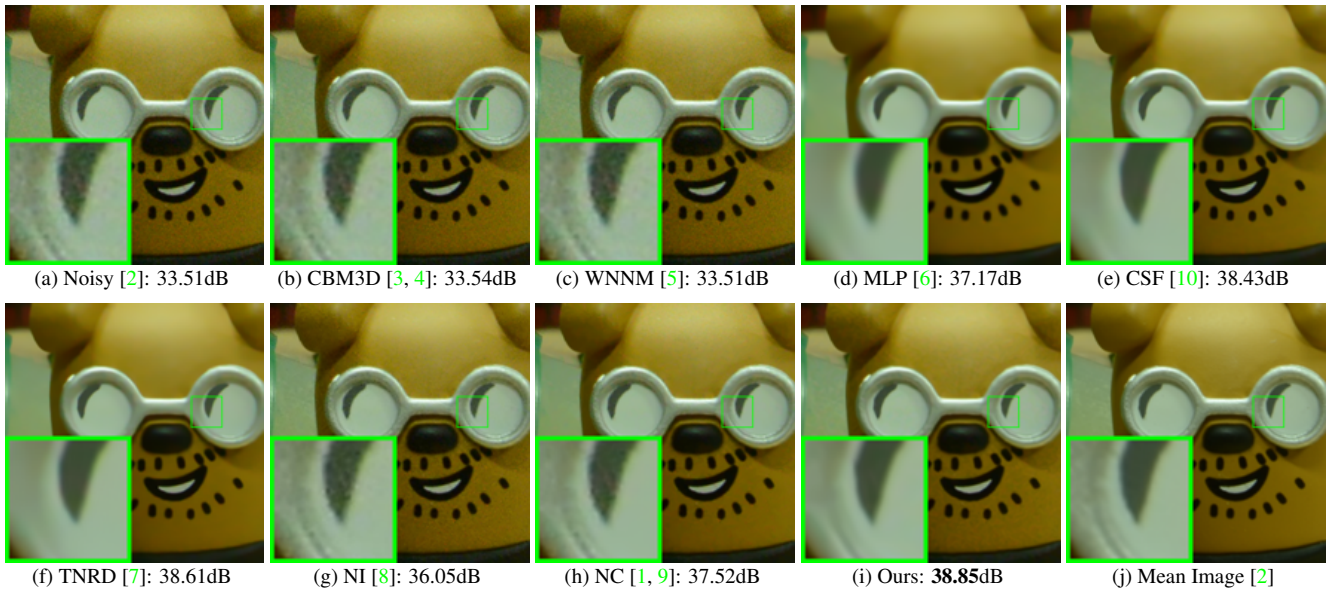


Figure 19. Denoised imagesupp of a region cropped from the real noisy image “Nikon D800 ISO 3200 A4” [2] by different methods. The images are better viewed by zooming in on screen.

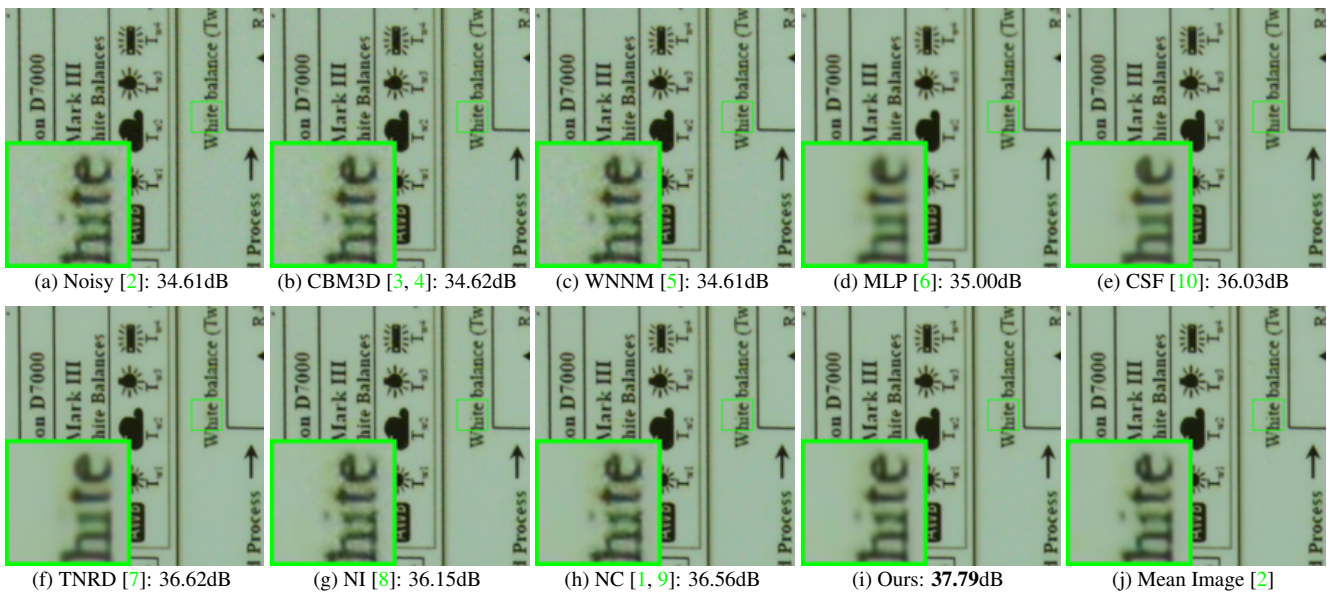


Figure 20. Denoised imagesupp of a region cropped from the real noisy image “Nikon D800 ISO 3200 A5” [2] by different methods. The images are better viewed by zooming in on screen.

## References

- [1] M. Lebrun, M. Colom, and J. M. Morel. The noise clinic: a blind image denoising algorithm. <http://www.ipol.im/pub/art/2015/125/>. Accessed 01 28, 2015. 1, 2, 3, 4, 5, 6, 7, 8, 9, 10, 11
- [2] S. Nam, Y. Hwang, Y. Matsushita, and S. J. Kim. A holistic approach to cross-channel image noise modeling and its application to image denoising. *IEEE Conference on Computer Vision and Pattern Recognition (CVPR)*, pages 1683–1691, 2016. 1, 3, 4, 5, 6, 7, 8, 9, 10, 11
- [3] K. Dabov, A. Foi, V. Katkovnik, and K. Egiazarian. Image denoising by sparse 3-D transform-domain collaborative filtering. *IEEE Transactions on Image Processing*, 16(8):2080–2095, 2007. 2, 3, 4, 5, 6, 7, 8, 9, 10, 11

- 1188 [4] K. Dabov, A. Foi, V. Katkovnik, and K. Egiazarian. Color image denoising via sparse 3D collaborative filtering with grouping  
1189 constraint in luminance-chrominance space. *IEEE International Conference on Image Processing (ICIP)*, pages 313–316, 2007. 2, 1242  
1190 3, 4, 5, 6, 7, 8, 9, 10, 11 1243  
1191 [5] S. Gu, L. Zhang, W. Zuo, and X. Feng. Weighted nuclear norm minimization with application to image denoising. *IEEE Conference*  
1192 *on Computer Vision and Pattern Recognition (CVPR)*, pages 2862–2869, 2014. 2, 3, 4, 5, 6, 7, 8, 9, 10, 11 1244  
1193 [6] H. C. Burger, C. J. Schuler, and S. Harmeling. Image denoising: Can plain neural networks compete with BM3D? *IEEE Conference*  
1194 *on Computer Vision and Pattern Recognition (CVPR)*, pages 2392–2399, 2012. 2, 3, 4, 5, 6, 7, 8, 9, 10, 11 1245  
1195 [7] Y. Chen, W. Yu, and T. Pock. On learning optimized reaction diffusion processes for effective image restoration. *IEEE Conference*  
1196 *on Computer Vision and Pattern Recognition (CVPR)*, pages 5261–5269, 2015. 2, 3, 4, 5, 6, 7, 8, 9, 10, 11 1246  
1197 [8] Neatlab ABSoft. Neat Image. <https://ni.neatvideo.com/home>. 2, 3, 4, 5, 6, 7, 8, 9, 10, 11 1247  
1198 [9] M. Lebrun, M. Colom, and J.-M. Morel. Multiscale image blind denoising. *IEEE Transactions on Image Processing*, 24(10):3149–  
1200 3161, 2015. 2, 3, 4, 5, 6, 7, 8, 9, 10, 11 1248  
1201 [10] U. Schmidt and S. Roth. Shrinkage fields for effective image restoration. *IEEE Conference on Computer Vision and Pattern Recog-*  
1202 *nition (CVPR)*, pages 2774–2781, June 2014. 6, 7, 8, 9, 10, 11 1249  
1203  
1204  
1205  
1206  
1207  
1208  
1209  
1210  
1211  
1212  
1213  
1214  
1215  
1216  
1217  
1218  
1219  
1220  
1221  
1222  
1223  
1224  
1225  
1226  
1227  
1228  
1229  
1230  
1231  
1232  
1233  
1234  
1235  
1236  
1237  
1238  
1239  
1240  
1241